Efficient cooperation of chloroplasts and mitochondria enhances ATP and sucrose production

Chia Pao Voon[1,†], Yee-Song Law[1,†], Xiaoqian Guan[1,†], Zhou Xu[1], Wing-Tung Chu[1], Renshan Zhang[1], Feng Sun[1], Mathias Labs[2,&], Mathias Pribil[2,‡], Dario Leister[2], Marie Hronková[3], Jiří Kubásek[3], Yong Cui[4,8], Liwen Jiang[4,8], Michito Tsuyama[5], Per Gardeström[6], Mikko Tikkanen[7], Boon Leong Lim[1,8*]

[1]School of Biological Sciences, the University of Hong Kong, Pokfulam, Hong Kong, China.
[2]Plant Molecular Biology, Department of Biology, Ludwig-Maximilians-University Munich (LMU), D-82152 Planegg-Martinsried, Germany.
[3]Faculty of Science, University of South Bohemia, Branisovska 31, 370 05 Ceske Budejovice, Czech Republic.
[4]School of Life Sciences, Centre for Cell and Developmental Biology, The Chinese University of Hong Kong, Shatin, Hong Kong, China.
[5]Department of Agriculture, Kyushu University, Fukuoka 812-8581, Japan.
[6]Umeå Plant Science Centre, Department of Plant Physiology, Umeå University, SE-901 87 Umeå, Sweden.
[7]Department of Biochemistry and Food Chemistry, Molecular Plant Biology, University of Turku, FI-20014 Turku, Finland.
[8]State Key Laboratory of Agrobiotechnology, The Chinese University of Hong Kong, Shatin, Hong Kong, China.

[†] These authors contributed equally to this work.
[*]Corresponding author: Boon Leong Lim (bllim@hku.hk); Tel.: (852) 22990826
[&] Current address: KWS SAAT SE, Gateway Research Center, St. Louis, MO, USA.
[‡] Current address: Copenhagen Plant Science Centre (CPSC), Department of Plant and Environmental Sciences, University of Copenhagen, Thorvaldsensvej 40, 1871 Frederiksberg C, Denmark.

Running title: Cooperation of chloroplasts and mitochondria

ABSTRACT

Efficient photosynthesis requires a balance of ATP and NADPH production/consumption in chloroplasts as the linear electron flow generates a higher NADPH/ATP ratio than that is consumed by the Calvin-Benson-Bassham cycle. Recent works suggested that ATP importation into mature chloroplasts of *Arabidopsis thaliana* is negligible, and therefore the exportation of reducing equivalents from chloroplasts is important for balancing stromal ATP/NADPH ratio. Here we showed that the overexpression of purple acid phosphatase 2 on the outer membranes of chloroplasts and mitochondria can streamline the production and consumption of reducing equivalents in these two organelles, respectively. A higher capacity of consumption of reducing equivalents in mitochondria can indirectly help chloroplasts to balance the ATP/NADPH ratio in stroma and recycle $NADP^+$, the electron acceptors of the linear electron flow. A higher rate of ATP and NADPH production from the linear electron flow, a higher capacity of carbon fixation by the Calvin-Benson-Bassham cycle and a greater consumption of NADH in mitochondria, enhance photosynthesis in the chloroplasts, ATP production in the mitochondria, sucrose synthesis in the cytosol, and eventually boosting plant growth and seed yields in the overexpression lines.

Keywords

Arabidopsis thaliana, ATP, AtPAP2, chloroplasts, mitochondria, NADPH, photosynthesis, photosystem

Significance Statement

This study demonstrates the importance of chloroplast-mitochondria cooperation in redox balance and illustrates that an optimized function of mitochondria can enhance the efficiency of photosynthesis.

Introduction

In plant cells, chloroplasts convert light energy into chemical energy, and mitochondria consume the chemical energy to produce ATP. The optimal carbon fixation and plant growth require these two energy-transforming organelles to perform strictly coordinated actions. Both organelles utilize protein complexes to construct electron transport chains (ETC), which are responsible for the formation (chloroplasts) or consumption (mitochondria) of reducing equivalents, translocation of protons, and the build-up of the proton gradient as a driving force for ATP synthesis. The cooperation between the chloroplasts and mitochondria, which was invented over 1.5 billion years ago, is nowadays much more complicated than the relationship between a supplier and a consumer in modern plant cells (Dutilleul et al., 2003; Noguchi and Yoshida, 2008). In chloroplasts, the linear electron flow (LEF) generates ATP/NADPH at a ratio of approximately 1.28, and the fixation of carbon dioxide consumes ATP/NADPH at a ratio of 1.5 (Allen, 2003; Foyer et al., 2012). Therefore, the photosynthetic efficiency requires the production and consumption of ATP and reductants at appropriate ratios in the chloroplasts, and this process is complicated by their fluxes across the chloroplast inner membrane. Our recent study showed that, in order to limit energy expenditure of chloroplasts in the dark, the import of cytosolic ATP into mature chloroplasts is negligible (Voon et al., 2018; Voon and Lim, 2019). Hence, during photosynthesis the ATP/NADPH ratio can either be balanced by extra ATP production from the cyclic electron flow (CEF) or the export of excess reductants to the cytosol (Sato et al., 2019; Selinski and Scheibe, 2019). In addition, photorespiration also generates a large amount of NADH in mitochondria and surplus reducing equivalents are exported to the cytosol through the malate-oxaloacetate (OAA) shuttle (Lim et al., 2020). Hence, surplus reducing equivalents generated during photosynthesis have to be stored as malate in the vacuole (Gerhardt et al., 1987). Light-dependent production of reducing equivalents in mitochondria is supported by the observation that illumination can cause a rapid pH change in the mitochondrial matrix, which was unseen when DCMU was applied (Voon et al., 2018). Furthermore, when the mitochondrial ETC was interfered by inhibitors, photosynthetic ATP production in stroma was also affected (Voon et al., 2018). Here, by studying the physiology of transgenic lines that overexpress *Arabidopsis thaliana* purple acid phosphatase 2 (AtPAP2), we showed that efficient cooperation of chloroplasts and mitochondria in optimizing reductant production in chloroplasts and consumption in chloroplasts and mitochondria is important for enhancing photosynthesis and productivity.

AtPAP2 is anchored on the outer membranes of chloroplasts and mitochondria and plays

a role in protein import into these two organelles (Law et al., 2015; Sun et al., 2012a; Zhang et al., 2016). The overexpression of AtPAP2 in *Arabidopsis thaliana* resulted in earlier bolting (Supplemental Fig. S1; Supplemental Video S1), a higher seed yield (+40-50%), and higher leaf sugar and ATP levels (Liang et al., 2015; Sun et al., 2013; Sun et al., 2012b). The overexpression of AtPAP2 also promotes plant growth and seed yield of the biofuel crop *Camelina sativa* (Zhang et al., 2012). Similarly to Toc33/34 and Tom20s, AtPAP2 is anchored onto the outer membranes of chloroplasts and mitochondria via its hydrophobic *C*-terminal motif (Sun et al., 2012a). AtPAP2 interacts with the precursor of the small subunit of RuBisCO (pSSU) (Zhang et al., 2016) and the presequences of a number of multiple organellar RNA editing factor (pMORF) proteins (Law et al., 2015) and plays a role in their import into chloroplasts (Zhang et al., 2016) and mitochondria (Law et al., 2015), respectively. Here, we examined how AtPAP2 overexpression affects the physiology of chloroplasts and mitochondria and how these two energy-generating organelles orchestrate to produce more sugars and ATP in leaf cells. Our data suggest that the efficiency of photosynthesis is dependent on the activities of the mitochondria. Surplus reducing equivalents generated from the LEF have to be exported and dissipated; and mitochondria that more actively dissipate the reducing equivalents can supply more ATP to the cytosol, thereby simultaneously relieving the pressure of over-reduction of ETC in the chloroplast (Scheibe et al., 2005). This streamlined cooperation enables a higher efficacy in carbon fixation, sucrose synthesis and ATP production in leaf cells.

Results

Overexpression of AtPAP2 changes the composition of the thylakoid membrane. Using transmission electron microscopy (TEM), alterations in the ultrastructure of the thylakoid membrane of mesophyll chloroplasts were observed in the OE lines (Fig. 1). The average diameters of the grana stacks were approximately 0.43 μm in all four lines, which is consistent with a previous report (Armbruster et al., 2013). Conversely, the average heights of the grana stacks in the OE7 and OE21 chloroplasts were smaller than the average heights of the grana stacks in the wild-type (WT) and *pap2* lines (Fig. 1). The decreased stacking may be due to the decreased amount of PSII (Fig. 2). An analysis of the photosynthetic pigments revealed that chlorophyll a, chlorophyll b, lutein and β-carotene were reduced in the two OE lines. The reduced chlorophyll content in the OE lines correlates with the reduction in the grana stacking. The level of violaxanthin was, however, unaltered, suggesting that the xanthophyll cycle in the OE plants was suppressed to minimize the thermal loss of the excitation energy (Supplemental

Table S1).

Overexpression of AtPAP2 changes the compositions of the photosystems and respiratory chain. 2D BN/SDS-PAGE DIGE revealed that the abundances of specific photosystem components were altered in the OE7 chloroplasts (Fig. 2A). The protein levels of the photosystem II (PSII) core proteins PsbC and PsbB were significantly reduced in OE7, while the abundances of the photosystem I (PSI) core proteins PsaA, PsaB, and PsaD were unaltered, implying that the PSI to PSII complex ratio is higher in the OE7 chloroplasts than that in the WT (Supplemental Table S2). The protein abundances of PsbO1 and RbcL (RuBisCO large subunit) were increased by at least 3-fold in the chloroplasts in the OE7 line. The ATP synthase complex subunits were significantly reduced in the OE7 line, including ATPA, ATPB, and ATPC (Supplemental Table S2). In the mitochondria, the protein abundances of the ATP synthase subunits alpha, beta and gamma were also lower in OE7 (Fig. 2B, Supplemental Table S3).

LEF, but not the CEF, was enhanced in the OE lines. To investigate the impact of the altered thylakoid composition on the photosynthetic performance, the photosynthetic electron transport in 20-day-old leaves was assessed using chlorophyll fluorescence analysis (Fig. 3). Both AtPAP2 OE lines displayed an increased PSII quantum yield Y(II), PSII photochemical capacity (qP), and electron transport rate (ETR) compared to the WT (Fig. 3A), which suggests that the OE lines exhibited a higher LEF efficiency. No difference in terms of absorptivity was observed between the WT and OE line, implying that the altered photosynthesis parameters in OE line was not due to any changes in chlorophyll absorption capacity (Supplemental Fig. S2). An analysis of the P700 redox state showed that the PSI in the OE lines was highly oxidized under low light conditions (25 – 125 μmol photon m^{-2} s^{-1}), suggesting that in the OE lines, the number of electrons that are captured from the PSI by downstream recipients (e.g., $NADP^{+}$) is higher than the number of electrons that is supplied by PSII to PSI (Fig. 3B). This phenomenon was not observed when the electron flow was larger at the higher light intensities. Although the ETR and P700 redox analysis suggested that the OE lines have a higher electron transfer capacity, the NAD(P)H dehydrogenase- and Fd- dependent CEF were not significantly changed in the OE lines according to the post-illumination chlorophyll fluorescence transient and ruptured chloroplast assay, respectively (Supplemental Fig. S3). In summary, the LEF, but not the CEF, was enhanced in the OE lines, and PSI played a key role in this enhancement by

relaying more electrons to $NADP^+$ in the transfer chain.

Photosynthesis rate was enhanced in the chloroplasts of the AtPAP2 OE lines. To study the effect of the altered thylakoid composition on the photosynthesis performance, the photosynthetic parameters were characterized in 20-day-old leaves by an analysis of gas exchange. Both OE lines exhibited a higher light-saturated-carbon fixation rate under ambient CO_2 concentration than the WT (Fig. 3C). This increased rate correlates with the higher abundance of RbcL in the OE chloroplasts (Fig. 2A). Assays of the Calvin-Benson-Bassham (CBB) cycle enzymes showed that the capacities of fructose bisphosphate aldolase and glyceraldehyde-3-phosphate dehydrogenase (GAPDH) were increased by 30 - 40% in the chloroplasts in the OE7 line (Table 1).

The mitochondria in the AtPAP2 OE line had a higher capacity in dissipating reducing equivalents. Reductant equivalents can be exported from the chloroplasts in the form of malate or DHAP (Shameer et al., 2019), which can be used for sucrose synthesis in the cytosol or converted to pyruvate and fed into the TCA cycle. Enzyme assays of the TCA cycle suggested that the OE7 mitochondria had an increased capacity of mitochondrial NAD^+-dependent malate dehydrogenase (mMDH) but not in the capacities of pyruvate dehydrogenase, citrate synthase or aconitase (Table 1), whereas the capacities of chloroplast $NADP^+$-dependent malate dehydrogenase, mMDH, 2-oxoglutarate dehydrogenase (2-OGDH), and succinyl-CoA synthetase were increased by 1.26-fold, 1.15-fold, 2.86-fold and 10.3-fold in the OE7 line, respectively. Our recent studies showed that glycine decarboxylase generates a large amount of NADH in mitochondria during photorespiration, which exceeds the NADH-dissipating capacity of the mitochondria. Consequently, the surplus NADH must be exported to the cytosol through the mitochondrial malate-OAA shuttle (Lim et al., 2020). The oxygraph studies showed that the electron-feeding capacities of complex II and internal NADH dehydrogenase, but not of complex I or external NADH dehydrogenase, were enhanced in the OE7 mitochondria (Table 2). If the OE line had a higher capacity in dissipating NADH, less surplus reducing equivalents will be exported to the cytosol through the malate-OAA shuttle.

Higher mitochondrial activity is responsible for the higher cytosolic ATP in the OE line. Our previous study showed that the leaf in the AtPAP2 OE lines contained a significantly higher level of ATP and a higher ATP/NADPH ratio in both dark and light conditions (Liang et al.,

2015). Here, we introduced a FRET $MgATP^{2-}$ sensor (Imamura et al., 2009; Voon et al., 2018) into the chloroplasts and the cytosol and a pH sensor (Schwarzländer et al., 2011) to the mitochondrial matrix and compared the responses of the OE7 and WT lines (Voon et al., 2018). Illumination led to an increased ATP concentration in the stroma (Fig. 4A) and alkalization of the mitochondrial matrix in both lines (Fig. 4B). The extent of the alkalization of the mitochondrial matrix was greater in the OE7 line than that in the WT, implying that under the same light intensity, the reducing power harvested by the chloroplasts may lead to a stronger proton translocation activity across the mitochondrial inner membrane (Fig. 4B). By contrast, the rate of increase in the ATP concentration in the stroma is lower in the OE7 line than that in the WT, which is likely due to a higher ATP consumption rate in the OE7 chloroplasts because the CO_2 fixation rate (Fig. 3C) and the capacities of certain CBB cycle enzymes are higher in the OE7 line (Table 1). We then examined the contribution of complex I, complex II and complex V in the OE7 mitochondria to cytosolic ATP. These inhibitors lower the cytosolic ATP in both lines (Fig. 4C). When complex I was inhibited by rotenone, the cytosolic ATP concentration was significantly higher in the OE7 line, suggesting that non-complex I activities in the OE7 mitochondria, such as complex II and internal NADH dehydrogenase, can compensate more effectively than those in the WT (Table 2). This difference was not observed when complex II was inhibited by TTFA. After one hour of incubation with oligomycin, cytosolic ATP in WT dropped to an undetectable level, whereas a higher level of cytosolic ATP was remained in OE7, suggesting that the intrinsic cytosolic ATP level was higher in OE7 than WT (Fig. 4C).

AtPAP2 selectively interacts with a number of chloroplast and mitochondrial proteins. A yeast two-hybrid (Y2H) library screening was carried out to identify other AtPAP2-interacting proteins. Forty nuclear-encoded AtPAP2-interacting proteins were identified; of these proteins, 32 and 3 proteins have been experimentally verified in chloroplasts and mitochondria, respectively (Supplemental Table S4). The other 5 AtPAP2-interacting proteins were predicted to be targeted to chloroplasts and/or mitochondria. AtPAP2 is exposed to the cytosolic side of the outer membrane of both organelles and its role in import of organellar proteins may account for the enrichment of nuclear-encoded organellar proteins. A systematic Y2H assay was then carried out to examine the interactions between AtPAP2 and various nucleus-encoded photosystem proteins (Supplemental Fig. S4A). AtPAP2 could specifically interact with Fd1, Fd2, PsaE2 (but not PsaE1), ferredoxin/thioredoxin reductase subunit A2 (FTRA2) (but not

191 FTRA1), FTRB, and photosynthetic NDH subcomplexes L1, L2, and L3 (PsbQ-like1, PsbQ-
192 like2, and PsbQ-like3). These interactions were verified by *in vivo* bimolecular fluorescence
193 complementation (BiFC) assays (Supplemental Fig. S4B and Supplemental Fig. S5). Hence,
194 AtPAP2 may play a role in the import of these precursor proteins, particularly the proteins at
195 the acceptor side of PSI, into chloroplasts.

196

Discussion

Maintenance of optimal photosynthetic efficiency requires the production and consumption of ATP and reductants in chloroplasts at appropriate ratios. Our recent study showed that the import of cytosolic ATP into mature chloroplasts of *Arabidopsis thaliana* is negligible and therefore could not supply additional ATP to the CBB cycle (Voon et al., 2018). Hence, the export of surplus reducing equivalents to extrachloroplast compartments is essential for balancing the ATP/NADPH ratio (Voon and Lim, 2019). Under illumination, the chloroplast is the producer of reducing equivalents and ATP, and the mitochondria consume the excess reducing equivalents to supply ATP to the cytosol (Gardeström and Igamberdiev, 2016; Shameer et al., 2019; Voon et al., 2018). The results presented here provide an example on how chloroplast function is highly dependent on the mitochondria. Illumination greatly elevates the amount of NADPH and the NADPH/ATP ratio in WT leaves (Liang et al., 2016), which represents a high reduction state in plant cells. Our previous studies showed that in the middle-of-day, the leaf sucrose and ATP contents are higher in the OE lines than those in the WT line in 20-day-old plants, whereas the leaf NADPH contents, NADPH/$NADP^+$ and NADPH/ATP ratios are lower in the OE lines than that in the WT line (Liang et al., 2015). Here, our data (Fig. 4, tables 1 and 2) indicated that the OE mitochondria may have a higher capacity to consume extra reducing equivalents to generate ATP (Fig. 5). This mechanism could account for the high ATP, high sucrose, but low NADPH content in the leaves of the OE lines in the middle-of-day (Liang et al., 2015; Sun et al., 2012b). In addition, the RuBisCO content (Fig. 2A) and the capacities of the CBB cycle enzymes FBA and GAPDH (Table 1) were higher in the OE chloroplasts. These could lead to a higher rate of CO_2 fixation (Fig. 3C) and a rapid recycling of ADP, $NADP^+$ and RuBP in the stroma. Hence, a faster recycling of ribulose-1,5-bisphosphate (RuBP) and an enhanced output of dihydroxyacetone phosphate (DHAP) from the OE chloroplasts could be achieved. This, together with a higher consumption rate of reductants by the mitochondria (Table 2), might cause a lower reduction state in the stroma, thereby leading to an enhancement of the LEF in the OE lines. This hypothesis is supported by our data from the P700 redox analysis (Fig. 3B). At low light conditions (25 – 125 µmol photon m^{-2} s^{-1}), in which the electron flow is smaller, PSI in the OE lines was highly oxidized, which was likely due to a high demand of electrons for the $NADP^+$ reduction or a higher PSI/PSII ratio (Fig. 2A and Supplemental Table S2). This oxidized state was relieved under higher light conditions (>125 µmol photon m^{-2} s^{-1}) when the electron flow was larger (Fig. 3B).

In pea (*Pisum sativum*), the PSI/PSII ratios were adjusted under different light conditions as follows: sunlight-grown, 0.55; yellow light (preferentially excites PSII), 0.40; and red light (preferentially excites PSI), 0.91 (Chow et al., 1990). Compared to plants with a lower PSI/PSII ratio, plants with a higher PSI/PSII exhibit a higher rate of oxygen evolution under illumination intensities that exceed 200 µmol photon m^{-2} s^{-1} (Chow et al., 1990). We also observed a higher PSI/PSII ratio in the OE chloroplasts than that in the WT chloroplasts in the 2D-DIGE analysis (Fig. 2A and Supplemental Table S2). The OE lines exhibited a higher ETR than the WT when the light intensity exceeded 200 µmol photon m^{-2} s^{-1} (Fig. 3). A higher PSI/PSII ratio allows for a faster throughput of electrons from the photosynthetic ETC via the PSI acceptor side and results in a lower possibility of an over-reduction in ETC (Tikkanen et al., 2014). Interestingly, the OE lines had also less stacked thylakoid membranes compared to the WT (Fig. 1). It is likely that the loose stacking increases the share of the grana margin domain that is composed of all components of the photosynthetic electron transfer chain in relation to the PSII-enriched grana stacks and PSI-enriched stroma lamellae. The importance of grana stacking for photosynthetic efficiency is not understood. Based on the results presented here, the loose stacking may be essential for the efficient interactions among the components of the photosynthetic electron transfer chain.

Consistently with this hypothesis, the analysis of the P700 (PSI reaction centre) redox state revealed that the P700 in the OE lines was relatively oxidized compared to that in the WT when the electron supply from PSII was limited (25 – 125 µmol photon m^{-2} s^{-1}) (Fig. 3B). Y2H showed that AtPAP2 preferably interacts with the downstream components of PSI, including PsaE2, Fd1, Fd2, FTRA2 and FTRB (Supplemental Fig. 4). Altogether, we hypothesize that the LEF rate in the OE lines was increased because of the higher capacity of electron transfer in PSI. LEF generates 1.28 mole ATP per mole of NADPH, but a minimum of 1.5 mole of ATP per mole of NADPH is required for carbon fixation (Allen, 2003; Foyer et al., 2012). It is generally believed that CEF pathways are needed to supplement ATP and modulate the ATP/NADPH ratio to meet the demand of metabolism (Foyer et al., 2012; Ishikawa et al., 2016). However, our studies showed that an enhancement of CEF is not required to support a more robust CBB cycle in the OE line (Supplemental Fig. S3). A recent study in diatom showed that the ATP generated from mitochondria can be transported to chloroplasts for carbon fixation (Bailleul et al., 2015), and it was believed that this also occurs in higher plants. However, our recent study showed that in the mesophyll of *Arabidopsis thaliana*, cytosolic ATP does not enter mature chloroplast to support carbon fixation (Voon et al., 2018). Altogether, because the

NADPH/ATP demand for carbon dioxide fixation is approximately 0.67, and a 0.77 molecule of NADPH is generated from each ATP molecule in LEF (Allen, 2003; Foyer et al., 2012), one could expect that a surplus reducing power is generated from LEF under illumination. Other metabolisms in chloroplasts, such as transcription and translation, also consume ATP molecules; therefore, the surplus of reducing equivalents would be more evident. The surplus of reducing equivalents must be exported and dissipated to recycle $NADP^+$ for efficient photosynthesis.

The reducing power generated from LEF can be exported as DHAP and malate (Fig. 5) (Noctor and Foyer, 2000; Scheibe, 2004). While modelling predicted that only 5% or less of the reducing equivalents from LEF can be exported through the malate-OAA shuttle (Fridlyand et al., 1998), the higher capacity of the NAD^+-MDH in the OE line might allow for the export of more reducing equivalents from the mitochondria to the cytosol through the malate-OAA shuttle. Illumination promotes the association between mitochondria and chloroplasts and peroxisomes (Oikawa et al., 2015), and, therefore, the malate-OAA shuttle can be a very efficient energy and reductant transfer pathway between the chloroplasts, mitochondria and peroxisomes. Malate and OAA in the stroma and cytosol were estimated to have concentrations ranging from 1 – 3 mM and 0.025-0.098 mM, respectively (Heineke et al., 1991). This concentration ratio is maintained by the large positive value of free energy change, Δ_fG, of malate dehydrogenation. This equilibrium can drive malate synthesis in the chloroplasts upon illumination because the chloroplast $NADP^+$-dependent malate dehydrogenase is activated by light (Scheibe, 1987; Zhao et al., 2018). The reducing power, thus, can be readily channelled to the peroxisomes for hydroxypyruvate reduction through the malate-OAA shuttle. As more reductants are consumed by the more active OE mitochondria, less exportation of reductants from mitochondria is expected. Hence, more reductants from the chloroplasts can be dissipated indirectly (Fig. 5). This is in line with our recent observation that the increase in stromal NADPH during illumination disappeared when photorespiration was absent (Abdel-Ghany, 2009; Lim et al., 2020).

In summary, the overexpression of AtPAP2 modulates the import of selected nucleus-encoded proteins into chloroplasts (Zhang et al., 2016) and mitochondria (Law et al., 2015), which leads to stronger sinks of reductants, including higher activities in the CBB cycle and mitochondrial ETC, in both organelles. A higher output of reducing equivalents from the LEF of chloroplasts (Fig. 3) and higher mitochondrial activities in utilizing the reducing equivalents for ATP production, thus, contribute to the higher ATP content and ATP/NADPH ratio in the OE lines (Liang et al., 2015). The simultaneous activation of chloroplasts and mitochondria is

295 required for the production of a surplus of ATP and sucrose; the transgenic lines that
296 overexpress AtPAP2 solely in the chloroplasts grew similarly to the WT (unpublished data),
297 and the transgenic lines that overexpress AtPAP2 solely in the mitochondria exhibited early
298 senescence and a lower seed yield (Law et al., 2015). These results provide an example of how
299 the efficient cooperation of chloroplasts and mitochondria can enhance ATP and sucrose
300 production in leaf cells. While AtPAP2 can enhance yield and growth in *Arabidopsis thaliana*,
301 it has negative impacts to plant survival. The OE lines are less resistant to drought and to *P.*
302 *syringae* infection (Zhang et al., 2017). Therefore, while AtPAP2-like genes were evolved from
303 green algae during evolution (Sun et al., 2012b), it may not be fully used by higher plants to
304 promote growth in natural environment, as survival is more important than high yield. It may
305 be more 'useful' for unicellular algae as water is never a constraint, and algae need to control
306 their growth rate and carbon level subject to the availability of P/N/Fe.
307 Over the past few decades, a controversy has emerged in the field regarding whether the
308 shortfall of ATP for the CBB cycle is fulfilled by the CEF or the import of ATP from the cytosol.
309 Combining the findings of our recent study (Voon et al., 2018) and this study, we concluded
310 that the efficient carbon fixation in the OE line is not dependent on an enhanced CEF or the
311 import of ATP from the cytosol to fulfil the shortfall of ATP generated from the LEF. Instead,
312 an efficient carbon fixation is dependent on an enhanced LEF, enhanced capacities of CBB
313 enzymes, the efficient export of surplus reducing equivalents from chloroplasts through the
314 malate-OAA shuttle and a higher reductant-dissipating activity of mitochondria. The ability of
315 mitochondria to dissipate reducing equivalents is important for relieving the built-up of surplus
316 reducing power in the stroma, which, in excess, will limit the LEF due to an insufficient supply
317 of $NADP^+$, the major electron acceptor of the LEF. Our recent studies showed that the reducing
318 equivalents from photorespiration are the major fuel for mitochondria in *Arabidopsis thaliana*
319 (Lim et al., 2020). The optimal use of reducing equivalents by mitochondria not only generates
320 more ATP for sucrose synthesis, but also reduces the export of reducing equivalents from the
321 mitochondria and therefore the overall redox status of the photosynthetic cells. This provides
322 a good example to illustrate the relationship between chloroplasts and mitochondria in
323 bioenergetics.
324

Methodology

Plant growth conditions. The WT *Arabidopsis thaliana* ecotype Columbia-o (WT), the *Arabidopsis thaliana* AtPAP2-overexpressing lines (OE7, OE21) and the *pap2* T-DNA insertion mutant (Salk_013567) (Sun et al., 2012b) were used in this study. *Arabidopsis* seeds were plated for 10 days on Murashige and Skoog (MS) medium, which was supplemented with 2% (w/v) sucrose. Seedlings of similar sizes were transferred to soil under growth chamber conditions (120-150 µmol m^{-2} s^{-1}, 16-h photoperiod, 22 °C).

Transmission electron microscopy (TEM). Plant materials (5th to 7th true leaves of 19-day-old plants at the beginning of the light period) were fixed with 2.5% (v/v) glutaraldehyde in 75 mM sodium cacodylate and 2 mM $MgCl_2$, pH 7.0, for 1 hour at 25 °C and post-fixed for 2 hours with 1% (w/v) osmium tetroxide in a fixative buffer at 25 °C. After two washing steps with distilled water, the pieces were dehydrated and then embedded in Spurr's low-viscosity resin. Ultrathin sections of 50–70 nm were cut with a diamond knife. The sections were post-stained with aqueous uranyl acetate/lead citrate. The TEM examination was performed under a Hitachi H-7650 transmission electron microscope with a charge-coupled device camera (Hitachi High-Technologies, Japan) operating at 80 kV.

Determination of the chlorophyll content using an HPLC analysis. Leaves (30-50 mg) were freeze-dried and extracted 3 times using 100% acetone (500 µl, 250 µl and 250 µl). The mixture was combined and centrifuged twice to eliminate the insoluble substances prior to the HPLC analysis. The pigment extract was separated and analysed (20 µL aliquots) on a Waters Spherisorb 5 µm ODS2 (4.6 × 250 mm) analytical column (Waters, USA) at room temperature. The fluids were eluted at a flow rate of 1.2 ml min^{-1} with a linear gradient from 100% solvent A [acetonitrile/methanol/0.1 M TRIS–HCl (pH 8.0), 84:2:14, v/v/v] to 100% solvent B (methanol/ethyl acetate, 68:32, v/v) over a 15-min period, followed by 10 min of 100% solvent B. The tridimensional chromatogram was recorded from 250 to 700 nm. The chromatographic peaks were identified by comparing the retention times and spectra to known standards provided by Sigma (USA) and Wako (Japan). The pigments were finally quantified by integrating the peak areas and converting them to concentrations according to the comparisons. The amounts of lutein, β−carotene, violaxanthin, chlorophyll a (Ca) and chlorophyll b (Cb) were calculated as follows: lutein: $Y = 2.56 \times 10^8 X - 153665$, $R = 0.99577$, $p < 0.0001$; β-

carotene: $Y = 6.57 \times 10^8 X - 61818$; violaxanthin: $Y = 2.68 \times 10^8 X + 236.6$; Chl a: $Y = 3.30 \times 10^7 X + 38832$; and Chl b: $Y = 7.31 \times 10^7 X + 29646$. Y = area, X = mg/ml.

2D Blue Native PAGE DIGE. Leaves from 20-day-old soil-grown WT and OE7 plants at the middle of the day (T = 8) were used as the starting materials. The chloroplast (Lamkemeyer et al., 2006) and mitochondria isolation (Lee et al., 2008) were performed as previously described. Cy Dye labelling of the chloroplast or mitochondrial proteins was carried out as previously described with modifications (Heinemeyer et al., 2009). In total, 100 µg chloroplast/mitochondrial proteins were centrifuged for 10 min at 4 °C at 1000 g using an Eppendorf centrifuge. The sedimented chloroplasts or mitochondria were re-suspended in a 10 µl solubilization buffer containing 30 mM HEPES, pH 7.4, 150 mM potassium acetate, 10% [v/v] glycerol, supplemented with 2% [w/v] beta-dodecyl maltoside (chloroplasts) or 5% [w/v] digitonin (mitochondria). The solubilized proteins were centrifuged for 20 min at 4 °C at full speed to remove the insoluble material. The supernatant containing the solubilized protein complexes was supplemented with 10 µl of the solubilization buffer containing 30 mM HEPES, pH 10, 150 mM potassium acetate, 10% [v/v] glycerol to adjust the pH value of the protein solution to approximately 8.5, which is a prerequisite for efficient labelling. Cy2, Cy3 and Cy5 NHS ester minimal dyes (Lumiprobe Corporation, USA) were reconstituted into 400 pmol/µl in DMF according to the manufacturer's instructions, and 2 µl of the Cy dye were added to the solubilized chloroplast or mitochondrial proteins. The WT was labelled using a Cy3 dye, and the OE was labelled with the Cy5 dye, while the internal standard (consisting of a pooled sample comprising an equal amount of all samples in the experiment) was labelled with Cy2. The labelling occurred for 30 min in the dark on ice and was stopped by adding 1 µl of a Lysine solution (10 mM). Finally, the sample was supplemented with 3 µl 5% (w/v) Serva Blue G (750 mM aminocaproic acid, 5% [w/v] Coomassie 250 G) and directly transferred into the slot of a blue native gel. The solubilized proteins were separated by two-dimensional Blue native/SDS PAGE as described previously by Wittig et al. (2006). The image acquisition was performed with a Typhoon Scanner, and the quantification of the Cy Dye labelled proteins resolved by the 2D Blue native PAGE was carried out using the SAMESPOTS software (Totallab, Tyne, England) based on the gel-images acquired from 3 biological replicates.

Chlorophyll *a* fluorescence measurement. The chlorophyll *a* fluorescence levels of the *Arabidopsis* leaves (20 days old) were monitored with IMAGING-PAM M-Series Maxi

Version (WALZ, Germany). The plants were dark-adapted for at least 1 hour before the measurements. After the maximum and initial fluorescence (F_m and F_0, respectively) were determined with a delay of 40 s, the plants were illuminated using the following light intensities: 0, 81, 145, 186, 281, 335, 461, 701, and 926 µmol photon m^{-2} s^{-1}. The duration of the illumination of each light intensity was 3 min. A saturation pulse (800 ms, 2700 µmol photon m^{-2} s^{-1}) was applied at the end of the 3-min illumination. For each light intensity, the photosynthesis parameters were calculated using the formulas: Y(II) was calculated as (Fm' – F) /Fm' ; qP is calculated as (Fm' – F) /(Fm' – Fo'); NPQ was calculated as (Fm – Fm') /Fm' ; ETR was calculated as Y(II) x light intensity x 0.5 x absorptivity. Fm' is the maximal fluorescence of light-illuminated plant. F is the current fluorescence yield. Fo' was estimated by Fo /(Fv /Fm + Fo /Fm') (Oxborough and Baker, 1997).

Measurements of CO_2 assimilation. The carbon dioxide assimilation in the 20-day-old plants was measured using the portable photosynthesis system LI-6400XT (LiCor, USA) and whole plant *Arabidopsis* chamber 6400-17. The plants were cultivated hydroponically in four- times diluted Hoagland nutrient solution (plants were fixed in "Grodan"-mineral wool cubes) under growth chamber conditions (irradiation 120-150 µmol m^{-2} s^{-1}, 16/8 h day/night photoperiod, temperature 22°C). The plants were transferred immediately before the measurement into conical pots dedicated to the 6400-17 chamber, and the boundary between the substrate (roots) and rosette was established using aluminium foil to minimize non-leaves transpiration. The light response of CO_2 assimilation was measured under ambient CO_2 concentration 400 µmol mol^{-1} and PAR levels 2000, 1000, 500, 250, 120, 60, 30, 15 and 0 µmol photon m^{-2} s^{-1}. Stable temperature at 25 °C and the relative air humidity between 50 and 70% were kept in the chamber during measurement.

Measurements of the post-illumination chlorophyll fluorescence transient. The modulated chlorophyll fluorescence was measured using a PAM 101 fluorometer (H. Walz, Germany). Before the minimal fluorescence (F_0) determination, the leaves were kept in darkness for at least 1 hour. The F_0 was induced by a red-modulated measuring light with a photon flux density (PFD) of approx. 0.2 µmol photon m^{-2} s^{-1}. The post-illumination Chl fluorescence increase is attributed to the back flow of electrons to the PQ pool from NADPH in the stroma via the cyclic electron flow around photosystem I (CEF-PSI), which depends on the NDH complex (Gotoh et al., 2010).

Ruptured chloroplast assay. The cyclic electron flow was measured in ruptured chloroplasts through an Fd-dependent plastoquinone reduction as previously described (Endo et al., 1998; Munekage et al., 2002). Briefly, the isolated chloroplasts (10 µg Chl) were osmotically ruptured in the analysis buffer (7 mM $MgCl_2$, 1 mM $MnCl_2$, 2 mM EDTA, 30 mM KCl, 0.25 mM KH_2PO_4, and 50 mM HEPES, pH 7.6) for 10 min prior to the analysis. One min after the initiation of the measurement, NADPH (Roche, Basel, Switzerland) was added to a final concentration of 0.25 mM. Maize ferredoxin (Sigma Aldrich, St. Louis, MO, USA) was added after an additional 30 s.

Enzyme assays of the Calvin-Benson-Bassham cycle and TCA cycle. The chloroplast proteins were used to assay the fructose 1,6-bisphosphate aldolase (Schaeffer et al., 1997) and $NADP^+$-glyceraldehyde-3-phosphate dehydrogenase activities. Enzyme assays of the TCA cycle were performed as described previously (Huang et al., 2015). The activity of the mitochondrial proteins (1-25 µg protein) were assayed spectrophotometrically using a Multiskan™ GO Microplate Spectrophotometer (Thermo Scientific, USA).

Measurements of oxygen consumption. A Clark-type oxygen electrode (Hansatech Instrument, UK) was used to measure oxygen consumption. The respiration rate of isolated mitochondria was measured at 25 °C in a chamber containing 1 ml of the respiration buffer (0.3 M Suc, 5 mM KH_2PO_4, 10 mM TES, 10 mM NaCl, 2 mM $MgSO_4$, and 0.1% [w/v] BSA, pH 6.8 or pH 7.2). The capacity of complex I, internal and external NADH dehydrogenases, and complex II were measured in the presence of deamino-NADH (1 mM), malate (10 mM), glutamate (10 mM), and NADH (1 mM) with or without ADP (100 µM) and/or rotenone (5 µM) as previously described (Jacoby et al., 2015; Meyer et al., 2009).

FRET-based ATP sensor and pH-dependent fluorescent probe. In the ATP sensor AT1.03, an ATP-binding epsilon-subunit of *Bacillus subtilis* F_oF_1-ATP synthase was fused between mseCFP and mVenus (Imamura et al., 2009). The binding of ATP changes the distance between mseCFP and mVenus and modulates the FRET signal (Imamura et al., 2009). The use of this sensor in plant systems was recently verified, and the chlorophyll fluorescence does not interfere with the FRET ratio in chloroplasts (Voon et al., 2018). To exclude the intensity contributed from sources other than the FRET signal, correction coefficients for bleed-through

and cross-excitation were determined separately in different plant compartments (Broussard et al., 2013). Sensitized FRET was used in all subsequent measurements involved AT1.03. To estimate the ATP concentration *in vivo*, sensitized FRET/ CFP ratios of purified recombinant AT1.03 sensor (6 μM) were calibrated with increasing ATP concentrations (0 – 6 mM) as previously described (Voon et al., 2018). A pH-dependent fluorescent probe with circularly permuted yellow fluorescent protein (cpYFP) was introduced into the matrix of the mitochondria (Nagai et al., 2001). cpYFP has a bimodal absorption spectrum with two peak maxima, 395 and 475 nm, and a single emission peak at 528 nm (Nagai et al., 2001). The absorption intensity of these two spectra is dependent on whether the chromophore of cpYFP is protonated or deprotonated. Protonated cpYFP displays a higher absorption at 395 nm, which emits a higher signal at 528 nm if excited at 395 nm. cpYFP was shown to response specifically to the pH value (Schwarzländer et al., 2011).

Yeast two-hybrid assay. A normalized yeast two-hybrid (Y2H) library was prepared from mRNAs that were isolated from eleven *Arabidopsis* tissues and was employed for the screening (Clontech Laboratories, Japan). The coding sequence of the mature bait protein AtPAP2 (25-613 a.a.), which lacks its signal peptide and C-terminal transmembrane motif, was fused to the C-terminus of the GAL4 DNA-binding domain (BD) in the pGBKT7 vector. The GAL4-based Y2H library screening was performed using the Matchmaker Gold Yeast Two-Hybrid System following the manufacturer's instructions (Clontech Laboratories, Japan). The mated culture was concentrated by centrifugation and spread onto agar plates (90 mm) containing triple dropout medium without Leu, Trp and His (TDO). Putative positive colonies (> 2 mm) were cultured on TDO liquid medium, and pGADT7 plasmids were extracted from the yeast cells for the *E. coli* transformation. The plasmids (pGADT7-prey) were re-extracted and sequenced. To identify the interactions between AtPAP2 and various components of the photosynthetic apparatus, the coding sequences of prey proteins were amplified from *Arabidopsis* leaf cDNA by Platinum™ *Pfx* polymerase (Thermo Scientific, USA) and fused downstream of the DNA-activating domain (AD) in the pGADT7 vector. The Y2HGold yeast cells were co-transformed with both the bait and prey protein constructs using the lithium acetate method and plated onto double dropout without Leu and Trp (DDO), TDO, and quadruple dropout without Ade, His, Leu and Trp (QDO) agar plates (Clontech Laboratories, Japan).

Bimolecular fluorescence complementation (BiFC). The full-length coding sequence of the

bait protein AtPAP2 was fused to the *C*-terminus of YFP^C in the pSPYCE vector, while the coding sequences of the photosynthetic apparatus subunits were fused to the N-terminus of the pSPYNE containing YFP^N (Kerppola, 2006). Both the prey and bait plasmids were transformed into the *Agrobacterium tumefaciens* strain GV3101, and the bacteria were infiltrated into the epidermal cell layers of tobacco leaves as previously described (Schweiger and Schwenkert, 2014). The transfected regions of the leaves were used for fluorescence detection after a 48-hour incubation in the dark under an LSM710 confocal laser scanning microscope (Zeiss). The primers that were used in this study are listed in Supplemental Table S5.

Acknowledgements

This project was supported by the Seed Funding Program for Basic Research (201311159043) of the University of Hong Kong, the General Research Fund (772012M) and the Area of Excellence Scheme (AoE/M-403/16) of the Hong Kong Research Grants Council, the Innovation and Technology Fund (Funding Support to State Key Laboratories in Hong Kong) of the HKSAR, China. Access to LI-6400 was supported by the Czech research infrastructure for systems biology C4SYS (project no LM2015055). We thank Prof. Wah Soon Chow and Dr. Maurice Cheung for their comments on this manuscript. We thank Dr. Huang Shaobai and Dr. Richard Jacoby for training of YL in enzyme assays, oxygraph and 2D-DIGE. We thank Prof. Hans-Peter Braun and Dr. Holger Eubel for technical advice in the 2D BN/SDS-PAGE DIGE analysis.

Authors' contributions

CPV, YL, and BLL wrote the manuscript with PG's input. CPV produced some of the transgenic sensor lines, performed the fluorescent sensor measurements, carried out the Maxi-Pam measurements and 2D BN-PAGE of the chloroplasts. YL carried out the 2D BN-PAGE of the mitochondria, the enzyme assays with WC, and the oxygraph assays with ZX. XG screened the yeast two-hybrid library and carried out the BiFC. RZ and FS produced the overexpression lines. FS measured the chlorophyll content. ML, MP and DL carried out the chloroplast rupture assay, MTik carried out the P700 assay, and MTsu carried out the post-illumination chlorophyll fluorescence. JK and MH carried out the CO_2 exchange measurements. YC and LJ carried out the TEM analysis. BLL coordinated this study. All authors read and approved the manuscript.

Competing financial interests.

AtPAP2 is the subject of US patent number 9,476,058.

521 **Supporting Information**

522 Supplemental Figure S1. The OE lines grew faster under both SD (8h/16h) and LD (16h/8h)
523 conditions.

524 Supplemental Figure S2. Leaf absorptivity is similar between WT line and AtPAP2
525 overexpression line (OE7).

526 Supplemental Figure S3. *In vivo* analysis of the cyclic electron flow rate.

527 Supplemental Figure S4. AtPAP2 selectively interacts with certain photosystem proteins.

528 Supplemental Figure S5. Results of BiFC negative controls.

529 Supplemental Table S1. Photosynthetic pigment content.

530 Supplemental Table S2. Chloroplast proteins identified in 2D BN PAGE.

531 Supplemental Table S3. Summary of identified mitochondrial protein spots.

532 Supplemental Table S4. AtPAP2-interacting proteins identified by Y2H library screening.

533 Supplemental Table S5. Primer list.

534

535 **References**

536 Abdel-Ghany, S.E. (2009) Contribution of plastocyanin isoforms to photosynthesis and
537 copper homeostasis in Arabidopsis thaliana grown at different copper regimes. *Planta* **229**,
538 767-779.
539 Allen, J.F. (2003) Cyclic, pseudocyclic and noncyclic photophosphorylation: new links in
540 the chain. *Trends in plant science* **8**, 15-19.
541 Armbruster, U., Labs, M., Pribil, M., Viola, S., Xu, W., Scharfenberg, M., Hertle, A.P.,
542 Rojahn, U., Jensen, P.E., Rappaport, F., Joliot, P., Dormann, P., Wanner, G. and Leister, D.
543 (2013) Arabidopsis CURVATURE THYLAKOID1 proteins modify thylakoid architecture by
544 inducing membrane curvature. *Plant Cell* **25**, 2661-2678.
545 Bailleul, B., Berne, N., Murik, O., Petroutsos, D., Prihoda, J., Tanaka, A., Villanova, V.,
546 Bligny, R., Flori, S., Falconet, D., Krieger-Liszkay, A., Santabarbara, S., Rappaport, F., Joliot,
547 P., Tirichine, L., Falkowski, P.G., Cardol, P., Bowler, C. and Finazzi, G. (2015) Energetic
548 coupling between plastids and mitochondria drives CO_2 assimilation in diatoms. *Nature* **524**,
549 366-369.
550 Broussard, J.A., Rappaz, B., Webb, D.J. and Brown, C.M. (2013) Fluorescence resonance
551 energy transfer microscopy as demonstrated by measuring the activation of the serine/threonine
552 kinase Akt. *Nat Protoc* **8**, 265-281.
553 Chow, W.S., Melis, A. and Anderson, J.M. (1990) Adjustments of Photosystem
554 Stoichiometry in Chloroplasts Improve the Quantum Efficiency of Photosynthesis. *Proc Natl*
555 *Acad Sci U S A* **87**, 7502-7506.
556 Dutilleul, C., Driscoll, S., Cornic, G., De Paepe, R., Foyer, C.H. and Noctor, G. (2003)
557 Functional mitochondrial complex I is required by tobacco leaves for optimal photosynthetic
558 performance in photorespiratory conditions and during transients. *Plant Physiol* **131**, 264-275.
559 Endo, T., Shikanai, T., Sato, F. and Asada, K. (1998) NAD(P)H dehydrogenase-dependent,
560 antimycin A-sensitive electron donation to plastoquinone in tobacco chloroplasts. *Plant and*
561 *Cell Physiology* **39**, 1226-1231.
562 Foyer, C.H., Neukermans, J., Queval, G., Noctor, G. and Harbinson, J. (2012)
563 Photosynthetic control of electron transport and the regulation of gene expression. *J Exp Bot*
564 **63**, 1637-1661.
565 Fridlyand, L.E., Backhausen, J.E. and Scheibe, R. (1998) Flux control of the malate valve
566 in leaf cells. *Arch Biochem Biophys* **349**, 290-298.
567 Gardeström, P. and Igamberdiev, A.U. (2016) The origin of cytosolic ATP in
568 photosynthetic cells. *Physiol Plantarum* **157**, 367-379.
569 Gerhardt, R., Stitt, M. and Heldt, H.W. (1987) Subcellular Metabolite Levels in Spinach
570 Leaves : Regulation of Sucrose Synthesis during Diurnal Alterations in Photosynthetic
571 Partitioning. *Plant Physiol* **83**, 399-407.
572 Gotoh, E., Matsumoto, M., Ogawa, K., Kobayashi, Y. and Tsuyama, M. (2010) A

qualitative analysis of the regulation of cyclic electron flow around photosystem I from the post-illumination chlorophyll fluorescence transient in Arabidopsis: a new platform for the in vivo investigation of the chloroplast redox state. *Photosynthesis research* **103**, 111-123.

Heineke, D., Riens, B., Grosse, H., Hoferichter, P., Peter, U., Flugge, U.I. and Heldt, H.W. (1991) Redox transfer across the inner chloroplast envelope membrane. *Plant Physiol* **95**, 1131-1137.

Heinemeyer, J., Scheibe, B., Schmitz, U.K. and Braun, H.P. (2009) Blue native DIGE as a tool for comparative analyses of protein complexes. *J Proteomics* **72**, 539-544.

Huang, S., Lee, C.P. and Millar, A.H. (2015) Activity assay for plant mitochondrial enzymes. *Methods Mol Biol* **1305**, 139-149.

Imamura, H., Nhat, K.P., Togawa, H., Saito, K., Iino, R., Kato-Yamada, Y., Nagai, T. and Noji, H. (2009) Visualization of ATP levels inside single living cells with fluorescence resonance energy transfer-based genetically encoded indicators. *Proc Natl Acad Sci U S A* **106**, 15651-15656.

Ishikawa, N., Takabayashi, A., Sato, F. and Endo, T. (2016) Accumulation of the components of cyclic electron flow around photosystem I in C4 plants, with respect to the requirements for ATP. *Photosynthesis research* **129**, 261-277.

Jacoby, R.P., Millar, A.H. and Taylor, N.L. (2015) Assessment of Respiration in Isolated Plant Mitochondria Using Clark-Type Electrodes. In: *Plant Mitochondria: Methods and Protocols* (Whelan, J. and Murcha, M.W. eds), pp. 165-185. New York, NY: Springer New York.

Kerppola, T.K. (2006) Design and implementation of bimolecular fluorescence complementation (BiFC) assays for the visualization of protein interactions in living cells. *Nature Protocols* **1**, 1278-1286.

Lamkemeyer, P., Laxa, M., Collin, V., Li, W., Finkemeier, I., Schottler, M.A., Holtkamp, V., Tognetti, V.B., Issakidis-Bourguet, E., Kandlbinder, A., Weis, E., Miginiac-Maslow, M. and Dietz, K.J. (2006) Peroxiredoxin Q of *Arabidopsis thaliana* is attached to the thylakoids and functions in context of photosynthesis. *Plant J* **45**, 968-981.

Law, Y.S., Zhang, R., Guan, X., Cheng, S., Sun, F., Duncan, O., Murcha, M., Whelan, J. and Lim, B.L. (2015) Phosphorylation and dephosphorylation of the presequence of pMORF3 during import into mitochondria from *Arabidopsis thaliana*. *Plant Physiol* **169**, 1-12.

Lee, C.P., Eubel, H., O'Toole, N. and Millar, A.H. (2008) Heterogeneity of the mitochondrial proteome for photosynthetic and non-photosynthetic Arabidopsis metabolism. *Molecular & cellular proteomics : MCP* **7**, 1297-1316.

Liang, C., Cheng, S., Zhang, Y., Sun, Y., Fernie, A.R., Kang, K., Panagiotou, G., Lo, C. and Lim, B.L. (2016) Transcriptomic, proteomic and metabolic changes in Arabidopsis thaliana leaves after the onset of illumination. *BMC Plant Biol* **16**, 43.

Liang, C., Zhang, Y., Cheng, S., Osorio, S., Sun, Y., Fernie, A.R., Cheung, C.Y.M. and

611 Lim, B.L. (2015) Impacts of high ATP supply from chloroplasts and mitochondria on the leaf
612 metabolism of *Arabidopsis thaliana*. *Front. Plant Sci.* **6**, 922.
613 Lim, S.L., Voon, C.P., Guan, X., Yang, Y., Gardestrom, P. and Lim, B.L. (2020) *In planta*
614 study of photosynthesis and photorespiration using NADPH and NADH/NAD^+ fluorescent
615 protein sensors. *Nature communications* **11**.
616 Meyer, E.H., Tomaz, T., Carroll, A.J., Estavillo, G., Delannoy, E., Tanz, S.K., Small, I.D.,
617 Pogson, B.J. and Millar, A.H. (2009) Remodeled respiration in ndufs4 with low
618 phosphorylation efficiency suppresses Arabidopsis germination and growth and alters control
619 of metabolism at night. *Plant Physiol* **151**, 603-619.
620 Munekage, Y., Hojo, M., Meurer, J., Endo, T., Tasaka, M. and Shikanai, T. (2002) PGR5
621 is involved in cyclic electron flow around photosystem I and is essential for photoprotection in
622 Arabidopsis. *Cell* **110**, 361-371.
623 Nagai, T., Sawano, A., Park, E.S. and Miyawaki, A. (2001) Circularly permuted green
624 fluorescent proteins engineered to sense Ca^{2+}. *Proc Natl Acad Sci U S A* **98**, 3197-3202.
625 Noctor, G. and Foyer, C.H. (2000) Homeostasis of adenylate status during photosynthesis
626 in a fluctuating environment. *J Exp Bot* **51**, 347-356.
627 Noguchi, K. and Yoshida, K. (2008) Interaction between photosynthesis and respiration
628 in illuminated leaves. *Mitochondrion* **8**, 87-99.
629 Oikawa, K., Matsunaga, S., Mano, S., Kondo, M., Yamada, K., Hayashi, M., Kagawa, T.,
630 Kadota, A., Sakamoto, W., Higashi, S., Watanabe, M., Mitsui, T., Shigemasa, A., Iino, T.,
631 Hosokawa, Y. and Nishimura, M. (2015) Physical interaction between peroxisomes and
632 chloroplasts elucidated by in situ laser analysis. *Nature Plants* **1**, 15035.
633 Oxborough, K. and Baker, N.R. (1997) Resolving chlorophyll a fluorescence images of
634 photosynthetic efficiency into photochemical and non-photochemical components –
635 calculation of qP and Fv-/Fm-; without measuring Fo. *Photosynthesis Research* **54**, 135-142.
636 Sato, R., Kawashima, R., Trinh, M.D.L., Nakano, M., Nagai, T. and Masuda, S. (2019)
637 Significance of PGR5-dependent cyclic electron flow for optimizing the rate of ATP synthesis
638 and consumption in Arabidopsis chloroplasts. *Photosynthesis research* **139**, 359-365.
639 Schaeffer, G.W., Sharpe, F.T. and Sicher, R.C. (1997) Fructose 1,6-bisphosphate aldolase
640 activity in leaves of a rice mutant selected for enhanced lysine. *Phytochemistry* **46**, 1335-1338.
641 Scheibe, R. (1987) Nadp+-Malate Dehydrogenase in C-3-Plants - Regulation and Role of
642 a Light-Activated Enzyme. *Physiol Plantarum* **71**, 393-400.
643 Scheibe, R. (2004) Malate valves to balance cellular energy supply. *Physiol Plantarum*
644 **120**, 21-26.
645 Scheibe, R., Backhausen, J.E., Emmerlich, V. and Holtgrefe, S. (2005) Strategies to
646 maintain redox homeostasis during photosynthesis under changing conditions. *J Exp Bot* **56**,
647 1481-1489.
648 Schwarzländer, M., Logan, D.C., Fricker, M.D. and Sweetlove, L.J. (2011) The circularly

permuted yellow fluorescent protein cpYFP that has been used as a superoxide probe is highly responsive to pH but not superoxide in mitochondria: implications for the existence of superoxide 'flashes'. *Biochem J* **437**, 381-387.

Schweiger, R. and Schwenkert, S. (2014) Protein-protein Interactions visualized by bimolecular fluorescence complementation in tobacco protoplasts and leaves. *Jove-J Vis Exp* **85**, e51327.

Selinski, J. and Scheibe, R. (2019) Malate valves: old shuttles with new perspectives. *Plant Biol (Stuttg)* **21**, 21-30.

Shameer, S., Ratcliffe, R.G. and Sweetlove, L.J. (2019) Leaf energy balance requires mitochondrial respiration and export of chloroplast NADPH in the light. *Plant Physiology* **180**, 1947-1961.

Sun, F., Carrie, C., Law, S., Murcha, M.W., Zhang, R., Law, Y.S., Suen, P.K., Whelan, J. and Lim, B.L. (2012a) AtPAP2 is a tail-anchored protein in the outer membrane of chloroplasts and mitochondria. *Plant signaling & behavior* **7**, 927-932.

Sun, F., Liang, C., Whelan, J., Yang, J., Zhang, P. and Lim, B.L. (2013) Global transcriptome analysis of AtPAP2--overexpressing *Arabidopsis thaliana* with elevated ATP. *Bmc Genomics* **14**, 752.

Sun, F., Suen, P.K., Zhang, Y., Liang, C., Carrie, C., Whelan, J., Ward, J.L., Hawkins, N.D., Jiang, L. and Lim, B.L. (2012b) A dual-targeted purple acid phosphatase in *Arabidopsis thaliana* moderates carbon metabolism and its overexpression leads to faster plant growth and higher seed yield. *The New phytologist* **194**, 206-219.

Tikkanen, M., Mekala, N.R. and Aro, E.M. (2014) Photosystem II photoinhibition-repair cycle protects Photosystem I from irreversible damage. *Bba-Bioenergetics* **1837**, 210-215.

Voon, C.P., Guan, X., Sun, Y., Sahu, A., Chan, M.N., Gardeström, P., Wagner, S., Fuchs, P., Nietzel, T., Versaw, W.K., Schwarzländer, M. and Lim, B.L. (2018) ATP compartmentation in plastids and cytosol of *Arabidopsis thaliana* revealed by fluorescent protein sensing. *Proc Natl Acad Sci U S A* **115**, 10778-10787.

Voon, C.P. and Lim, B.L. (2019) ATP translocation and chloroplast biology *National Science Review* **6**, 1073-1076.

Wittig, I., Braun, H.P. and Schagger, H. (2006) Blue native PAGE. *Nat Protoc* **1**, 418-428.

Zhang, R., Guan, X., Law, Y.S., Sun, F., Chen, S., Wong, K.B. and Lim, B.L. (2016) AtPAP2 modulates the import of the small subunit of Rubisco into chloroplasts. *Plant signaling & behavior* **11**, e1239687.

Zhang, R., Qi, H., Sun, Y., Xiao, S. and Lim, B.L. (2017) Transgenic Arabidopsis thaliana containing increased levels of ATP and sucrose is more susceptible to *Pseudomonas syringae*. *PLoS One* **12**, e0171040.

Zhang, Y., Yu, L., Yung, K.F., Leung, D.Y., Sun, F. and Lim, B.L. (2012) Over-expression of AtPAP2 in *Camelina sativa* leads to faster plant growth and higher seed yield. *Biotechnology*

for biofuels **5**, 19.

Zhao, Y.N., Luo, L.L., Xu, J.S., Xin, P.Y., Guo, H.Y., Wu, J., Bai, L., Wang, G.D., Chu, J.F., Zuo, J.R., Yu, H., Huang, X. and Li, J.Y. (2018) Malate transported from chloroplast to mitochondrion triggers production of ROS and PCD in *Arabidopsis thaliana*. *Cell Res* **28**, 448-461.

Figure Legends

Figure 1. Comparison of the thylakoid architecture between the WT and OE plants. TEM micrograph of ultrathin sections of 20-day-old leaves from the WT, OE (OE7 and OE21) and AtPAP2 knock-out (*pap2*) lines. Average value (n>30) of the diameter (nm) and height (nm) of the thylakoid in the WT and OE lines were shown. Values marked by different letters in the same column are significantly different ($p < 0.05$) by Student's t-test. The diameter (nm) and height (nm) of WT chloroplasts isolated from 28-day-old leaves in another study (15) were 448 ± 16 nm and 113 ± 5 nm, respectively.

Figure 2. Comparative analysis of the chloroplast and mitochondrial proteomes of WT and OE7 plants. **A**. Chloroplasts; **B**. Mitochondria. Proteins from the WT fraction were pre-labelled with Cy3; proteins from the OE fraction were pre-labelled with Cy5. Combined protein fractions were separated by 2D Blue-native/SDS-PAGE, and the protein visualization was carried out by laser scanning at the respective wavelengths using the Typhoon laser scanner. On the resulting overlay image, Cy3 is represented by red, and Cy5 is represented by green. Proteins with a reduced abundance in the OE7 line are shown in red; proteins with an increased abundance in the OE7 line are shown in green; and proteins of equal abundance in the two compared fractions are shown in yellow. Protein spots were extracted and identified by an MS/MS analysis. Identified proteins with the highest unused score and at least 2 unique peptides (95%) were labelled with the corresponding spot ID (Supplemental Tables S2 & S3). The representative gel images of 3 biological replicates are presented.

Figure 3. *In vivo* analysis of the electron transport activity and CO_2 assimilation rate. A. Light intensity-dependent NPQ, qP, ETR and Y(II). The 3-week-old plants were dark-acclimated for 1 hour before the measurement. Data are presented as the mean ± SE ($n > 10$ per line). **B**. P700 Oxidation. Data are presented as the mean ± SD ($n = 3$ per line). Light intensity was increased in a step-wise manner as stated in the graph. **C**. Light response of CO_2 assimilation rates (An) under ambient CO_2 concentration. Data are presented as the mean ± SE ($n = 5$ per line). The asterisks indicate significant differences between the WT and both OE lines by one-way ANOVA with post-hoc Tukey HSD test ($p < 0.05$).

Figure 4. Assessing organelle activities using fluorescent sensors. A. Change in apparent $MgATP^{2-}$ concentration in the chloroplast stroma. 10-day-old WT and OE7 cotyledon

expressing TKTP-AT1.03 were illuminated (296 µmol photon m^{-2} s^{-1}) for 3 mins, followed by 5 mins in the dark. **B**. Changes in the mitochondrial matrix pH sensor ratio (Ex 488/ Ex 405). 10-day-old WT and OE7 cotyledon expressing matrix-localized pH sensor, mt-cpYFP were illuminated (296 µmol photon m^{-2} s^{-1}) for 30 s, followed by 1 min in the dark. Black and white bars indicate the dark and illumination periods, respectively. Average value of 6 independent measurements and SE are shown. The asterisks indicate significant differences between the WT and the OE line by one-way ANOVA with post-hoc Tukey HSD test ($p < 0.05$). Graphs were normalized to the initial point. **C**. Effects of the inhibitors on cytosolic ATP concentration. Inhibitors of complex I (50 µM rotenone), complex II (100 µM TTFA) and complex V (10µM oligomycin) were applied to 10-day-old WT and OE7 seedling expressing C-AT1.03 seedlings by vacuum infiltration for 5 min. Before the measurements, the seedlings were incubated in the dark for 1 hour. Average value of 3 replicates is presented. Error bars are the standard error of the average $MgATP^{2-}$ concentration. Groups with significant difference by one-way ANOVA with post-hoc Tukey HSD test ($p < 0.05$) are indicated by different letters. The dashed line indicates the maximal $MgATP^{2-}$ concentration (1.4 mM) that can be reported by AT1.03 (Voon et al., 2018). The groups marked by asterisks are significantly different from the groups marked by letters but whether they have intergroup differences are not known.

Figure 5. A model on how efficient collaboration between chloroplasts and mitochondria promote ATP and sucrose production. ① and ② AtPAP2 on the outer membranes of chloroplasts and mitochondria promotes the import of certain proteins into these two organelles via the Toc or the Tom complexes. ③ Higher PSI/PSII ratio and higher LEF generate more NADPH and ATP at a ratio of 0.78, which are consumed at a ratio of 0.67 by the enhanced CBB enzymes in the OE chloroplasts for CO_2 fixation. The surplus reducing equivalents are exported from the chloroplasts via the malate/OAA shuttle to recycle $NADP^+$ as the electron acceptors of the LEF. ④ Higher reductant-dissipating activities of OE mitochondria reduce the needs for mitochondria to export reductants from photorespiration in the form of malate. ⑤ OE chloroplasts with enhanced rate of carbon fixation export more carbon skeletons to the cytosol. ⑥ OE mitochondria with higher reductant-dissipating activities generate more ATP through the respiratory electron transfer (RET) chain. ⑦ Higher ATP production in OE mitochondria and higher output of carbon skeletons from chloroplasts enhance sucrose synthesis in the cytosol. Red and blue lines indicate upregulated and downregulated pathways/metabolites in the OE lines, respectively.

Table 1. Enzyme activities of the CBB cycle and the Krebs cycle.

Table 2 Respiration rates of different complexes of WT and OE7 mitochondria.

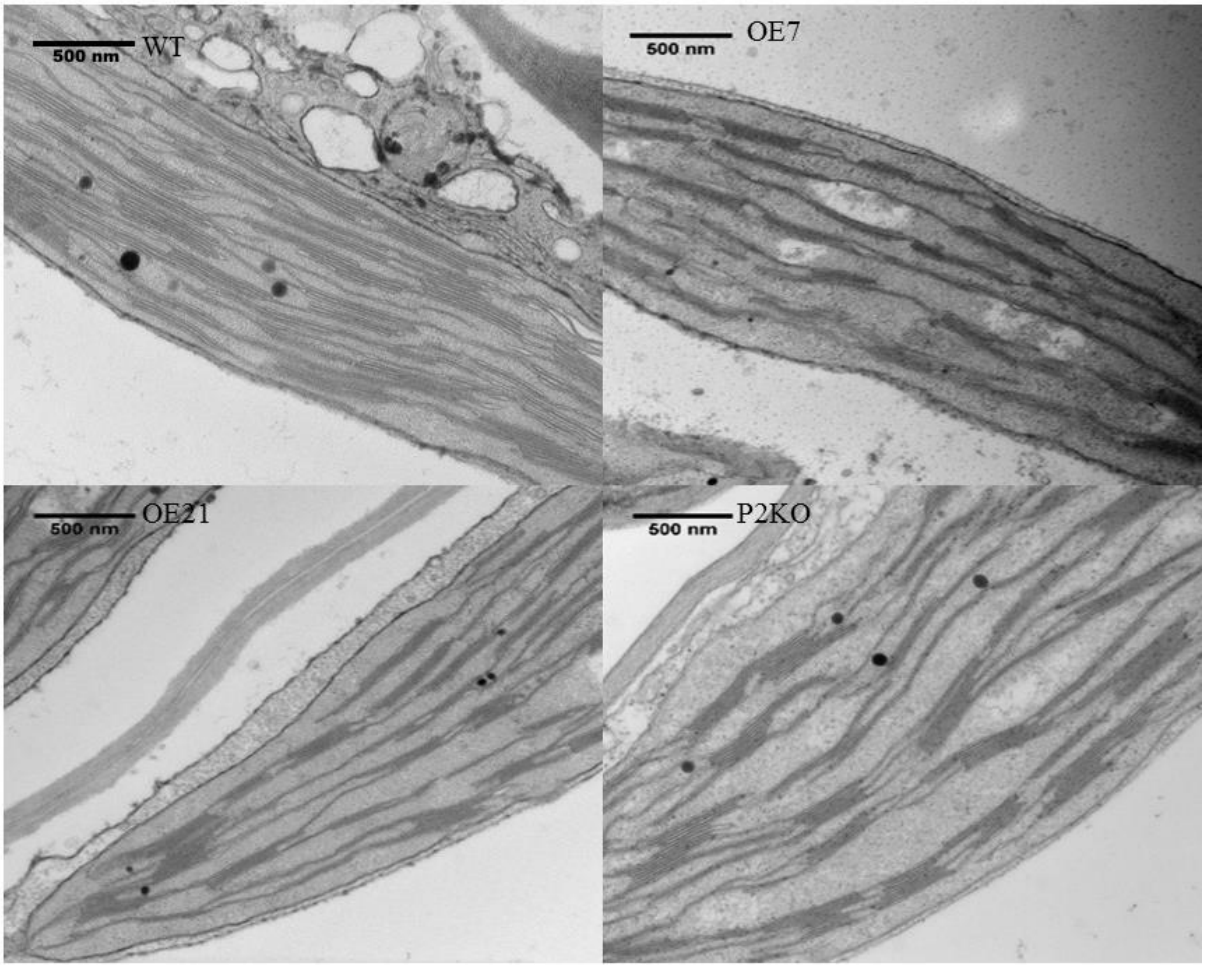

Mean ± SEM	Diameter (nm)	Height (nm)
WT	432 ± 19 [a]	125 ± 8 [a]
pap2	444 ± 11[a]	102 ± 5[b]
OE7	431 ± 16 [a]	78 ± 4[c]
OE21	430 ± 12 [a]	79 ± 3[c]

Figure 1. Comparison of the thylakoid architecture between the WT and OE plants. TEM micrograph of ultrathin sections of 20-day-old leaves from the WT, OE (OE7 and OE21) and AtPAP2 knock-out (*pap2*) lines. Average value (n>30) of the diameter (nm) and height (nm) of the thylakoid in the WT and OE lines were shown. Values marked by different letters in the same column are significantly different ($p < 0.05$) by Student's t-test. The diameter (nm) and height (nm) of WT chloroplasts isolated from 28-day-old leaves in another study (15) were 448 ± 16 nm and 113 ± 5 nm, respectively.

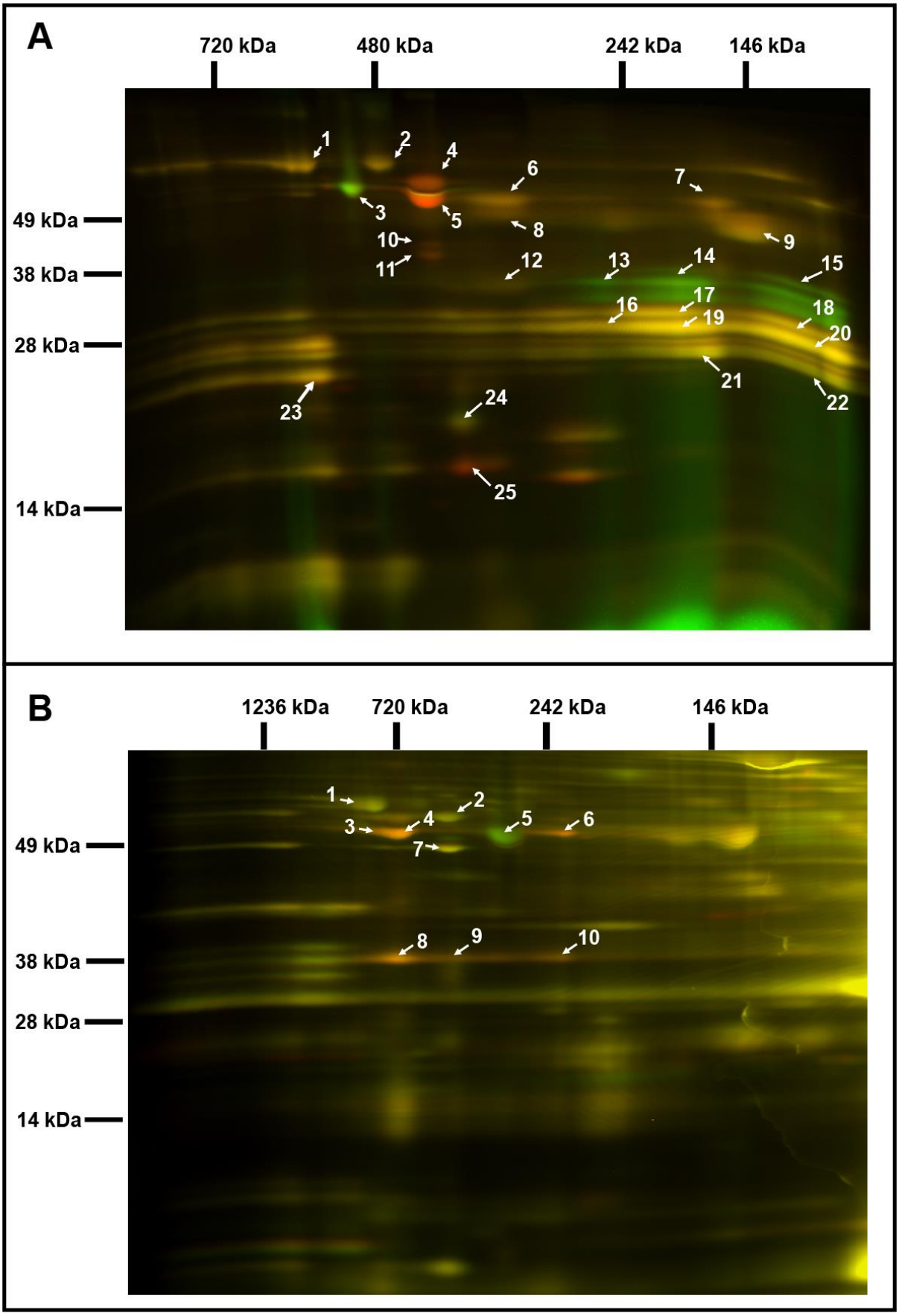

Figure 2. Comparative analysis of the chloroplast and mitochondrial proteomes of WT

and OE7 plants. **A**. Chloroplasts; **B**. Mitochondria. Proteins from the WT fraction were pre-labelled with Cy3; proteins from the OE fraction were pre-labelled with Cy5. Combined protein fractions were separated by 2D Blue-native/SDS-PAGE, and the protein visualization was carried out by laser scanning at the respective wavelengths using the Typhoon laser scanner. On the resulting overlay image, Cy3 is represented by red, and Cy5 is represented by green. Proteins with a reduced abundance in the OE7 line are shown in red; proteins with an increased abundance in the OE7 line are shown in green; and proteins of equal abundance in the two compared fractions are shown in yellow. Protein spots were extracted and identified by an MS/MS analysis. Identified proteins with the highest unused score and at least 2 unique peptides (95%) were labelled with the corresponding spot ID (Supplemental Tables S2 & S3). The representative gel images of 3 biological replicates are presented.

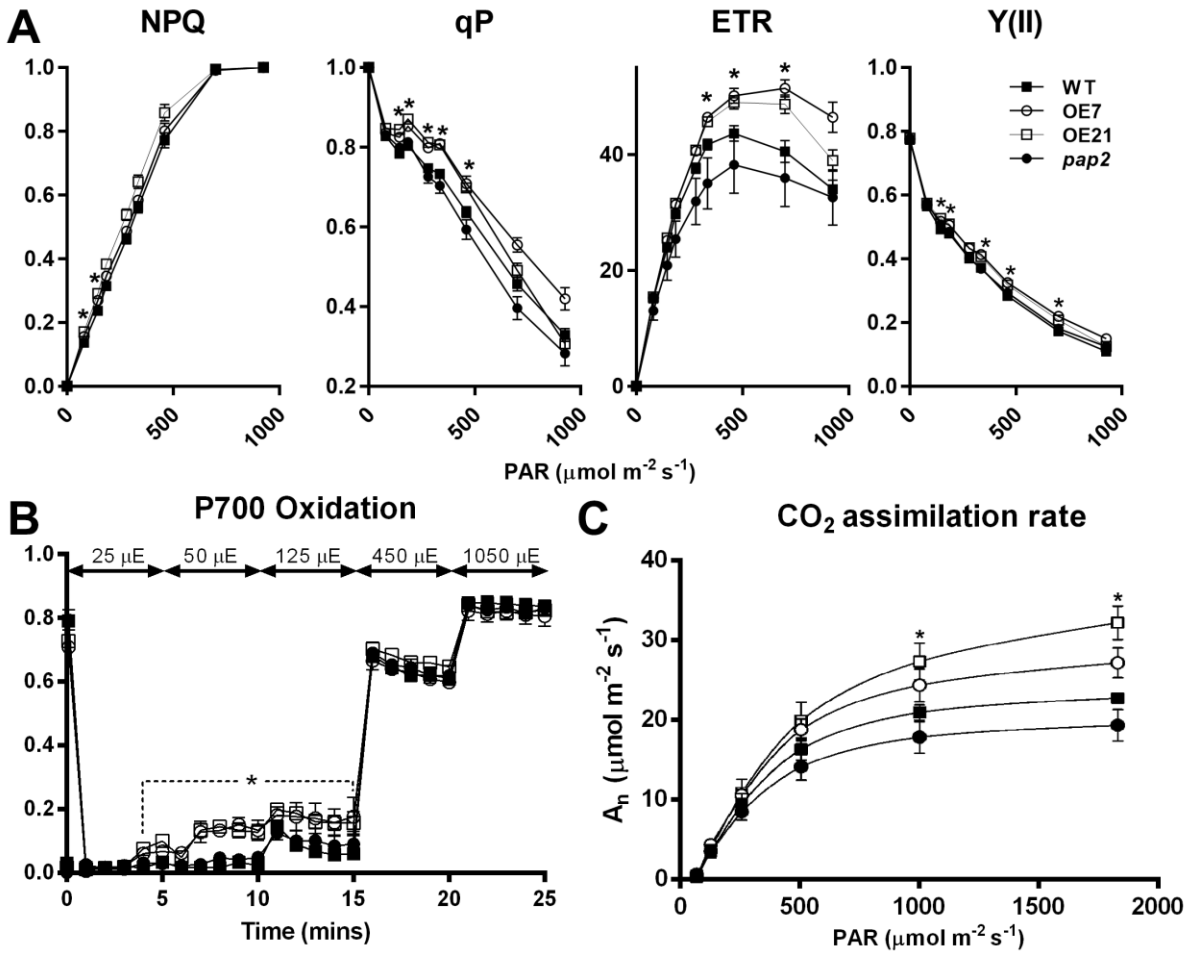

Figure 3. ***In vivo*** **analysis of the electron transport activity and CO_2 assimilation rate. A**. Light intensity-dependent NPQ, qP, ETR and Y(II). The 3-week-old plants were dark-acclimated for 1 hour before the measurement. Data are presented as the mean ± SE (n > 10 per line). **B**. P700 Oxidation. Data are presented as the mean ± SD (n = 3 per line). Light intensity was increased in a step-wise manner as stated in the graph. **C**. Light response of CO_2 assimilation rates (An) under ambient CO_2 concentration. Data are presented as the mean ± SE (n = 5 per line). The asterisks indicate significant differences between the WT and both OE lines by one-way ANOVA with post-hoc Tukey HSD test ($p < 0.05$).

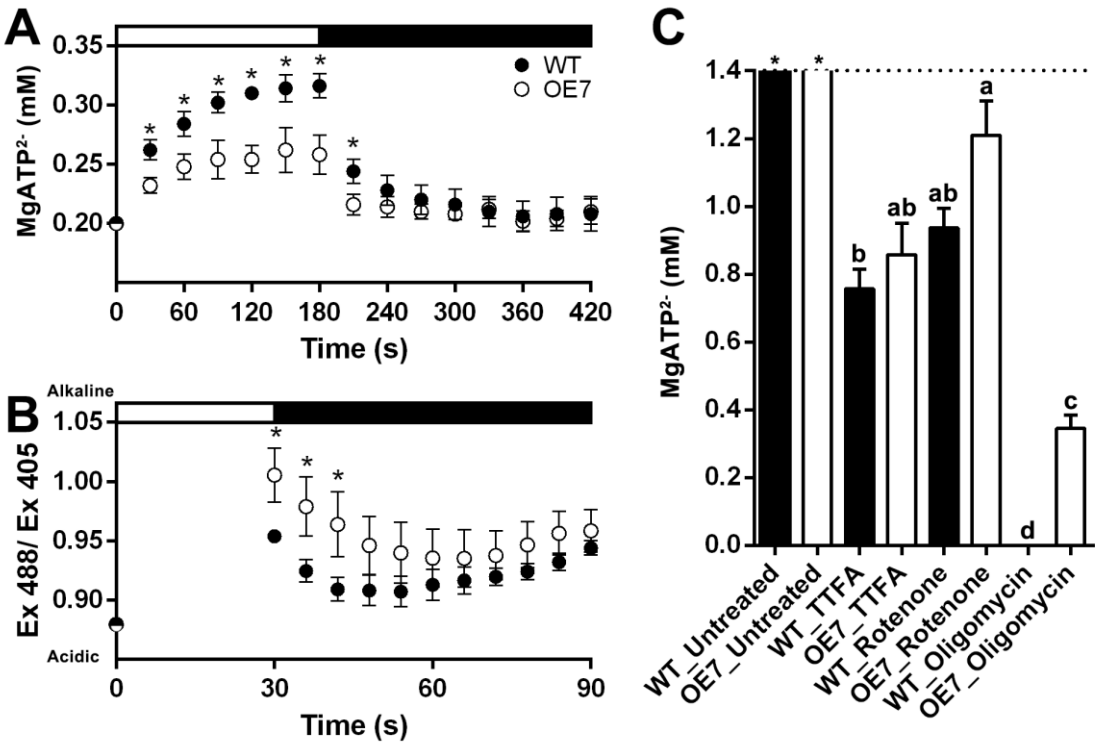

Figure 4. Assessing organelle activities using fluorescent sensors. A. Change in apparent $MgATP^{2-}$ concentration in the chloroplast stroma. 10-day-old WT and OE7 cotyledon expressing TKTP-AT1.03 were illuminated (296 µmol photon m^{-2} s^{-1}) for 3 mins, followed by 5 mins in the dark. **B**. Changes in the mitochondrial matrix pH sensor ratio (Ex 488/ Ex 405). 10-day-old WT and OE7 cotyledon expressing matrix-localized pH sensor, mt-cpYFP were illuminated (296 µmol photon m^{-2} s^{-1}) for 30 s, followed by 1 min in the dark. Black and white bars indicate the dark and illumination periods, respectively. Average value of 6 independent measurements and SE are shown. The asterisks indicate significant differences between the WT and the OE line by one-way ANOVA with post-hoc Tukey HSD test ($p < 0.05$). Graphs were normalized to the initial point. **C**. Effects of the inhibitors on cytosolic ATP concentration. Inhibitors of complex I (50 µM rotenone), complex II (100 µM TTFA) and complex V (10µM oligomycin) were applied to 10-day-old WT and OE7 seedling expressing C-AT1.03 seedlings by vacuum infiltration for 5 min. Before the measurements, the seedlings were incubated in the dark for 1 hour. Average value of 3 replicates is presented. Error bars are the standard error of the average $MgATP^{2-}$ concentration. Groups with significant difference by one-way ANOVA with post-hoc Tukey HSD test ($p < 0.05$) are indicated by different letters. The dashed line indicates the maximal $MgATP^{2-}$ concentration (1.4 mM) that can be reported by AT1.03 (Voon et al., 2018). The groups marked by asterisks are significantly different from the groups marked by letters but whether they have intergroup differences are not known.

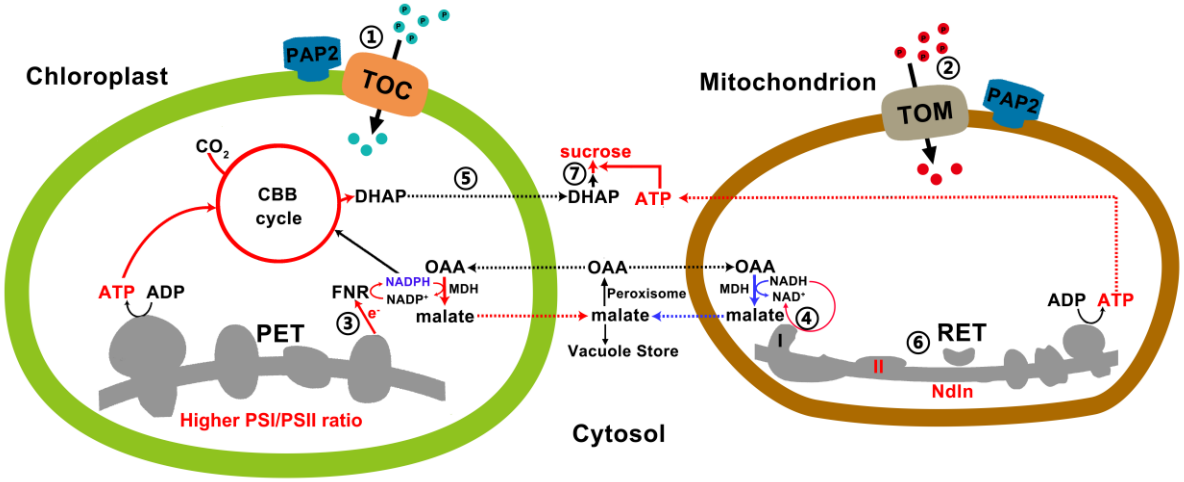

Figure 5. A model on how efficient collaboration between chloroplasts and mitochondria promote ATP and sucrose production. ① and ② AtPAP2 on the outer membranes of chloroplasts and mitochondria promotes the import of certain proteins into these two organelles via the Toc or the Tom complexes. ③ Higher PSI/PSII ratio and higher LEF generate more NADPH and ATP at a ratio of 0.78, which are consumed at a ratio of 0.67 by the enhanced CBB enzymes in the OE chloroplasts for CO_2 fixation. The surplus reducing equivalents are exported from the chloroplasts via the malate/OAA shuttle to recycle $NADP^+$ as the electron acceptors of the LEF. ④ Higher reductant-dissipating activities of OE mitochondria reduce the needs for mitochondria to export reductants from photorespiration in the form of malate. ⑤ OE chloroplasts with enhanced rate of carbon fixation export more carbon skeletons to the cytosol. ⑥ OE mitochondria with higher reductant-dissipating activities generate more ATP through the respiratory electron transfer (RET) chain. ⑦ Higher ATP production in OE mitochondria and higher output of carbon skeletons from chloroplasts enhance sucrose synthesis in the cytosol. Red and blue lines indicate upregulated and downregulated pathways/metabolites in the OE lines, respectively.

824 **Table 1. Enzyme activities of the CBB cycle and the Krebs cycle.**

Enzyme	Source	WT	OE	Change
Fructose bisphosphate aldolase	Chloroplast	92 ± 8	123 ± 14**	1.34X
$NADP^+$-GAPDH	Chloroplast	97 ± 11	138 ± 4**	1.42X
$NADP^+$-MDH	Chloroplast	328 ± 20	413 ± 40**	1.26X
$NADP^+$-MDH	Leaf	26 ± 4	28 ± 4	N.S.
NAD^+-MDH	Leaf	1525 ± 25	1439 ± 39	N.S.
NAD^+-MDH	Mitochondria	4657 ± 206	5354 ±46**	1.15X
NAD^+-malic enzyme, ME	Mitochondria	40 ± 3	42 ± 3	N.S.
Pyruvate dehydrogenase, PDC	Mitochondria	45 ± 6	48 ± 4	N.S.
Citrate synthase, CS	Mitochondria	84 ± 12	90 ± 12	N.S.
Aconitase, ACN	Mitochondria	314 ± 18	322 ± 18	N.S.
NAD^+-ICDH	Mitochondria	43 ± 3	63 ± 8**	1.47X
$NADP^+$-ICDH	Leaf	18.5 ± 2.2	6.7 ± 0.5**	0.36X
2-oxoglutarate dehydrogenase, 2OGDH	Mitochondria	1.4 ± 0.6	4.0 ± 0.4**	2.86X
Succinate dehydrogenase, SDH	Mitochondria	7.6 ± 0.3	10.3 ± 1.0**	1.35X
Succinyl-CoA synthetase	Mitochondria	29 ± 1.4	300 ± 63**	10.3X
Fumarase, FUM	Mitochondria	334 ± 55	209 ± 34**	0.62X

825 *GAPDH*, glyceraldehyde-3-phosphate dehydrogenase; *ICDH*, isocitrate dehydrogenase; *MDH*, malate
826 dehydrogenase. All enzyme unit is presented as nmol/min/mg protein.
827 Independent sample t-test was carried out. Significant differences between WT and OE7 are showed by asterisks.
828 * $p < 0.05$, ** $p < 0.01$, n=4. N.S.: Not significant.
829

Table 2 Respiration rates of different complexes of WT and OE7 mitochondria.

Enzyme	Substrate	ADP	Rotenone	WT	OE7	Change
Complex I	deamino-NADH	-	-	30 ± 6	33 ± 5	ns
		-	+	8 ± 3	8 ± 5	ns
Complex II	Succinate	-	-	49 ± 3	48 ± 23	ns
		+	-	75 ± 4	92 ± 10 *	1.23X
NdEx	NADH	-	-	45 ± 4	45 ± 12	ns
		+	-	65 ± 4	68 ± 4	ns
NdIn	Malate + Glutamate	-	+	39 ± 4	46 ± 6	ns
		+	+	64 ± 8	85 ± 4 *	1.32X

Oxygen consumption rates of complex I (rotenone-sensitive deamino-NADH oxidation), complex II, external NADH dehydrogenase, internal NADH dehydrogenase (rotenone-insensitive NADH oxidation) were expressed as nmol min^{-1} mg^{-1} protein.

* indicates statistically significant difference ($p < 0.05$, $n \geq 3$) and ns indicates not significant difference between WT and OE7 by Student's t test.